

AD-A193 634

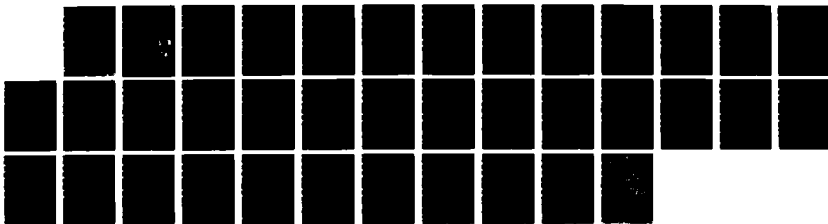
ABSORPTION SPECTRA AND ENERGY LEVELS OF GD(3+) ND(3+)
AND CR(3+) IN THE GARNET GD3SC2GA3O12(U) HARRY DIAMOND
LABS ADELPHI MD J B GRUBER ET AL MAR 88 HDL-TR-2116

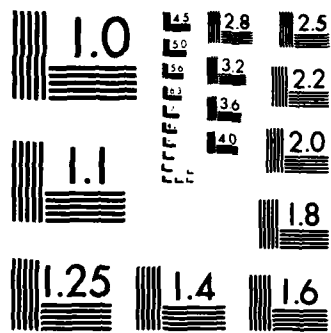
1/1

UNCLASSIFIED

F/G 7/2

NL





MICROCOPY RESOLUTION TEST CHART
NATIONAL BUREAU OF STANDARDS-1963-A



AD-A193 634

HDL-TR-2136

March 1988

Absorption Spectra and Energy Levels of Gd^{3+} , Nd^{3+} , and Cr^{3+} in the Garnet $Gd_3Sc_2Ga_3O_{12}$

by John B. Gruber
Marian E. Hills
Clyde A. Morrison
Gregory A. Turner
Milan R. Kokta

DTIC
ELECTE
APR 18 1988
S E D
E



U.S. Army Laboratory Command
Harry Diamond Laboratories
Adelphi, MD 20783-1197

Approved for public release; distribution unlimited.

88 4 15 094

The findings in this report are not to be construed as an official Department of the Army position unless so designated by other authorized documents.

Citation of manufacturers' or trade names does not constitute an official endorsement or approval of the use thereof.

Destroy this report when it is no longer needed. Do not return it to the originator.

UNCLASSIFIED

SECURITY CLASSIFICATION OF THIS PAGE

REPORT DOCUMENTATION PAGE				Form Approved OMB No 0704-0188 Exp Date Jun 30 1986	
1a REPORT SECURITY CLASSIFICATION UNCLASSIFIED		1b RESTRICTIVE MARKINGS			
2a SECURITY CLASSIFICATION AUTHORITY		3 DISTRIBUTION/AVAILABILITY OF REPORT Approved for public release; distribution unlimited.			
2b DECLASSIFICATION/DOWNGRADING SCHEDULE					
4 PERFORMING ORGANIZATION REPORT NUMBER(S) HDL-TR-2136		5 MONITORING ORGANIZATION REPORT NUMBER(S)			
6a NAME OF PERFORMING ORGANIZATION Harry Diamond Laboratories	6b OFFICE SYMBOL (if applicable) SLCHD-ST-RA	7a NAME OF MONITORING ORGANIZATION			
6c ADDRESS (City, State, and ZIP Code) 2800 Powder Mill Road Adelphi, MD 20783-1197		7b ADDRESS (City, State, and ZIP Code)			
8a NAME OF FUNDING/SPONSORING ORGANIZATION Center for Night Vision & Electro-Optics	8b OFFICE SYMBOL (if applicable)	9 PROCUREMENT INSTRUMENT IDENTIFICATION NUMBER			
8c ADDRESS (City, State, and ZIP Code) Fort Belvoir, VA 22060		10 SOURCE OF FUNDING NUMBERS			
		PROGRAM ELEMENT NO 61102A	PROJECT NO	TASK NO	WORK UNIT ACCESSION NO
11 TITLE (Include Security Classification) Absorption Spectra and Energy Levels of Gd ³⁺ , Nd ³⁺ , and Cr ³⁺ in the Garnet Gd ₃ Sc ₂ Ga ₃ O ₁₂					
12 PERSONAL AUTHOR(S) John B. Gruber, Marian E. Hills, Clyde A. Morrison, Gregory A. Turner, and Milan R. Kokta (see reverse)					
13a TYPE OF REPORT Interim	13b TIME COVERED FROM Oct 86 To June 87	14 DATE OF REPORT (Year, Month, Day) March 1988	15 PAGE COUNT 34		
16 SUPPLEMENTARY NOTATION AMS code: 611102.31B0011; PRON: CJ727269-01-CJ-CT; HDL Project: 590751					
17 COSATI CODES		18 SUBJECT TERMS (Continue on reverse if necessary and identify by block number)			
FIELD	GROUP	SUB-GROUP			
20	02		Spectra, rare earth, gadolinium, neodymium, chromium, transition metal, crystalfield theory ←		
20	05				
19 ABSTRACT (Continue on reverse if necessary and identify by block number)					
<p>Absorption spectra recorded between 0.3 and 6.7 μm are reported for trivalent gadolinium, trivalent neodymium, and trivalent chromium in single-crystal gadolinium scandium gallium garnet, Gd₃Sc₂Ga₃O₁₂, at liquid helium, liquid nitrogen, and room temperatures. Crystalline electric-field-split energy levels are established from data between 1,500 and 35,000/cm² for Gd³⁺ (4f⁷), Nd³⁺ (4f³), and Cr³⁺ (3d³). The Gd³⁺ and Nd³⁺ ions occupy sites having D₂ point symmetry; Cr³⁺ ions are found primarily in sites of C_{3v} point symmetry. A Hamiltonian consisting of Coulombic, spin-orbit, and crystalline electric-field terms, having symmetry appropriate to each ion, is diagonalized to obtain theoretical energy levels. The rms deviation between calculated and observed levels for Nd³⁺ (with 45 levels) is 1.7/cm², for Gd³⁺ (with 14 levels) is 4/cm², and for Cr³⁺ (with 35 levels) is 87.7/cm². A lattice sum calculation is compared with the phenomenological parameters obtained from fitting the observed energy levels.</p>					
20 DISTRIBUTION/AVAILABILITY OF ABSTRACT <input checked="" type="checkbox"/> UNCLASSIFIED/UNLIMITED <input type="checkbox"/> SAME AS RPT <input type="checkbox"/> DTIC USERS		21 ABSTRACT SECURITY CLASSIFICATION UNCLASSIFIED			
22a NAME OF RESPONSIBLE INDIVIDUAL Clyde A. Morrison		22b TELEPHONE (Include Area Code) (202) 394-2042	22c OFFICE SYMBOL SLCHD-ST-RA		

DD FORM 1473, 84 MAR

83 APR edition may be used until exhausted
All other editions are obsolete

SECURITY CLASSIFICATION OF THIS PAGE

UNCLASSIFIED

UNCLASSIFIED

SECURITY CLASSIFICATION OF THIS PAGE

12. PERSONAL AUTHORS (cont'd)

John Gruber—San Jose State University
Marian E. Hills—Naval Weapons Center
Clyde A. Morrison and Gregory A. Turner—Harry Diamond Laboratories
Milan R. Kokta—Union Carbide Corporation

Accession For	
NTIS	<input checked="" type="checkbox"/>
GRA&I	<input type="checkbox"/>
DTIC TAB	<input type="checkbox"/>
Unannounced	<input type="checkbox"/>
Justification	
By	
Distribution/	
Availability Codes	
Dist	Avail and/or Special
A-1	

COPY INSPECTED 4

UNCLASSIFIED

SECURITY CLASSIFICATION OF THIS PAGE

Contents

	Page
1. Introduction	5
2. Experimental Results	7
3. Results and Conclusions	9
3.1 Observed Spectra	9
3.2 Crystal-Field Splitting Calculations: Nd^{3+} , Gd^{3+}	20
3.3 Crystal-Field Splitting Calculations: Cr^{3+}	22
4. Conclusions	27
References	27
Distribution	31

Figures

1. Absorption spectrum of $[4I]11/2$ manifold of Nd^{3+} recorded at liquid helium temperature with FTIR spectrometer	12
2. Absorption spectrum of $[4I]13/2$ manifold of Nd^{3+} recorded at liquid helium temperature with FTIR spectrometer	12
3. Absorption spectrum of $[4F]3/2$ manifold of Nd^{3+} recorded at room temperature showing temperature-dependent transitions from Stark levels Z_2 (106 cm^{-1}), Z_3 (167 cm^{-1}), and Z_4 (263 cm^{-1}) of ground state manifold $[4I]9/2$	12
4. Absorption spectrum of Cr^{3+} levels 3 through 10 and the $[4F]9/2$ manifold (B group) of Nd^{3+} recorded at liquid helium temperature	17
5. Absorption spectrum of $[2H]11/2$ manifold of Nd^{3+} superimposed on first strong Cr^{3+} band, recorded at liquid helium temperature	17

Figures (cont'd)

6. Absorption spectrum of $\text{Cr}^{3+}:\text{GSGG}$ between 3000 and 8000 Å recorded at room temperature with a Cary Model 17 spectrophotometer 18
7. Absorption spectrum of $[4D]3/2$ (*L* group), $[4D]5/2$ and $[2I]11/2$ (*M* group), and part of $[4D]7/2$ and $[2I]13/2$ (*N* group) manifolds of Nd^{3+} superimposed on third Cr^{3+} band recorded at liquid helium temperature 18
8. Absorption spectrum of $[6P]7/2$ (*A* group), $[6P]5/2$ (*B* group), and $[6P]3/2$ (*C* group) manifolds of Gd^{3+} recorded at room temperature 19

Tables

1. Infrared energy levels: Nd^{3+} 11
2. Visible and ultraviolet energy levels: Nd^{3+} 13
3. Absorption spectra of Cr^{3+} at liquid helium temperature 16
4. Ultraviolet energy levels: Gd^{3+} 19
5. Crystallographic and x-ray data of $\text{Gd}_3\text{Sc}_2\text{Ga}_3\text{O}_{12}$ 20
6. CEF parameters for Nd^{3+} and Gd^{3+} 22

1. Introduction

In recent years gadolinium scandium gallium garnet, $\text{Gd}_3\text{Sc}_2\text{Ga}_3\text{O}_{12}$ (GSGG), has received growing attention as a laser host material [1-11]. The luminescence and stimulated emission from trivalent neodymium in GSGG were first reported by Kaminskii and coworkers [1]. Struve et al [2] observed broad fluorescence from GSGG doped with trivalent chromium. They were able to demonstrate Cr^{3+} laser action in their crystals. Several groups [3-7] discovered that co-doping GSGG with Nd^{3+} and Cr^{3+} resulted in more efficient energy transfer to the Nd^{3+} energy levels involved in laser action. The spectroscopic, optical, and thermomechanical properties of $\text{Nd}^{3+}:\text{Cr}^{3+}:\text{GSGG}$ recently reported by Krupke and coworkers [11] suggest potential for this material as a powerful laser.

Several years ago we began a theoretical analysis of the crystalline electric field (CEF) splitting of the energy levels of trivalent neodymium, gadolinium, and chromium in GSGG [12-14]. At that time only the experimental CEF splitting of the $[4I]J$ and $[4F]3/2$ manifolds of trivalent neodymium had been reported [1,15,16]. Recently Struve and Huber [17] published their work on the energy levels, line broadening, and transition probabilities based on the optical spectra of $\text{Cr}^{3+}:\text{GSGG}$. Using as an approximation the cubic energy level scheme of Sugano and Tanabe [18,19], they concluded that the 4T_2 level is admixed into the 2E level via spin-orbit coupling [20]. However, no CEF-splitting calculations addressing the correct symmetry for Cr^{3+} , Nd^{3+} , or Gd^{3+} in GSGG have been reported.

This paper presents the absorption spectra and energy levels for Gd^{3+} , Nd^{3+} , and Cr^{3+} in GSGG up to $35,000\text{ cm}^{-1}$ recorded at liquid helium, liquid nitrogen, and room temperatures. The CEF-splitting calculations for Gd^{3+} , Nd^{3+} , and Cr^{3+} are based on the complete diagonalization of a Hamiltonian including Coulombic, spin-orbit, and CEF terms in symmetry appropriate to the trivalent ion site. The diagonalization involves the 11 lowest $4f^3 [SL]J$ manifolds for Nd^{3+} and the 12 lowest $4f^7 [SL]J$ manifolds for Gd^{3+} . The assumption is made that Nd^{3+} substitutes into Gd^{3+} sites of D_2 point symmetry in the garnet lattice. The CEF-splitting calculation for trivalent chromium assumes that the ions substitute into scandium (C_{3i}) sites. Analyses of fluorescence data [17] and vibronic spectra

are used to establish CEF levels of Cr^{3+} since zero-phonon electronic electric-dipole transitions are forbidden between $3d^3$ states at ion sites having inversion symmetry. The complete diagonalization of the $3d^3$ states in a strong crystalline electric field of C_{3i} symmetry with spin-orbit interaction yields energy levels and wavefunctions different from those obtained from the Sugano and Tanabe calculations for cubic symmetry with no spin-orbit corrections [18,19].

2. Experimental Results

Single crystals were grown parallel to the $\langle 111 \rangle$ direction by the Czochralski technique. The starting chemicals were all 99.999 percent pure. An indium crucible 3 in. in diameter and 3 in. deep was used. The crystal was rotated at 15 rpm and pulled at 0.015 in./hr. The growth was carried out under an atmosphere of N_2 containing 2-percent O_2 by volume; O_2 is added in order to minimize the evaporation of gallium during growth. The resulting boule was 1.5 in. in diameter and 6 in. long. A section for optical measurement was cut perpendicular to the growth axis from the center portion of the boule, where the calculated concentrations were 1.56 at. wt. % neodymium based on gadolinium and 1.2 at. wt. % chromium based on scandium.

GSGG is a garnet derivative of gadolinium garnet (GGG) where octahedrally coordinated gallium is replaced with scandium. The critical growth behavior of GSGG very closely resembles that of GGG. There are, however, some minute differences as may be expected. The congruent GGG composition, with which the crystals grow, contains 1 at. wt. % gadolinium ions in octahedral sites (based on octahedral gallium) as is evidenced by comparison of lattice parameters-- a (GGG) = 12.376 Å and a (congruent GGG) = 12.384 Å.* Such "spillover" of gadolinium into octahedral sites is not the case in GSGG. The doping of GSGG with neodymium and chromium is better controlled as compared with $Y_3Al_5O_{12}$ (YAG). The dopant distribution is governed by the same principles, but the distribution coefficients are much more favorable to uniform doping. The neodymium distribution coefficient $K = 0.6$, and the chromium distribution coefficient approaches unity very closely. This results in only a very small variation of neodymium concentration in the crystal, and the chromium distribution is uniform.

The Ca^{2+} impurity concentration was below 3 ppm by weight of scandium oxide. This is very important with respect to the absorption spectrum of Cr^{3+} in garnets, because the presence of divalent calcium affects the absorption of chromium in garnets by changing relative intensities of the $^4A_2 \rightarrow ^4T_2$ and $^4A_2 \rightarrow ^4T_1$ transitions, as well as introducing a broad absorption feature in the region of 0.90 to 1.2 μm . The nature of this effect is

*(\AA) + 10 = (nm).

not yet explained. The crystal grown for this work contained such small Ca^{2+} concentration that its effect may be neglected.

Absorption spectra recorded between 6000 and 1500 cm^{-1} with a resolution of 0.5 cm^{-1} were obtained from a Nicolet Model 7199 Fourier transform infrared (FTIR) spectrometer. Data were also recorded between 35,000 and 4,000 cm^{-1} using a Cary Model 17D spectrophotometer. In the ultraviolet region the accuracy of the instrument is about 3 Å and the resolution is better than 2 Å. Some examples of this resolution are found in the figures representing the observed splitting of the $[6P]J$ manifolds of Gd^{3+} in the ultraviolet. The precision in measuring the separation between peaks associated with a given manifold at a given temperature is better than 0.2 Å. In the region of overlap between the spectrophotometer and the FTIR spectrometer, the agreement is within one wavenumber.

A conduction dewar was used to obtain spectra at liquid nitrogen and liquid helium temperatures. Sample temperatures were not measured; the spectra were recorded no sooner than 30 minutes after the dewar was filled to allow for thermal equilibration.

3. Results and Conclusions

3.1 Observed Spectra

Below 1700 cm^{-1} the garnet lattice absorbs [14-16]. Between 1700 and 6000 cm^{-1} the only absorption found is associated with the $[4I]11/2$, $[4I]13/2$, and $[4I]15/2$ manifolds of Nd^{3+} . Temperature-dependent spectra were used to establish the excited Stark levels of the ground state manifold $[4I]9/2$ of Nd^{3+} as follows: $Z_2 = 106\text{ cm}^{-1}$, $Z_3 = 167\text{ cm}^{-1}$, and $Z_4 = 264\text{ cm}^{-1}$. Table 1 lists the experimentally established energy levels in the near-infrared region obtained from an analysis of spectra recorded at three different temperatures. The energy levels are similar, with few exceptions, to those derived for fluorescence data by Kaminskii and his coworkers for $\text{Nd}^{3+}:\text{GSGG}$ at liquid nitrogen temperature [1].

The absorption spectrum of the $[4I]11/2$ and $[4I]13/2$ manifolds of Nd^{3+} at liquid helium temperature is shown in figures 1 and 2. A sharp relatively weak peak appears to the low-energy side of peaks Y_1 , Y_2 , Y_3 , X_1 , and X_3 . Peak X_4 in figure 2 has an unresolved shoulder on each side. The weak peaks are found within 3 to 8 cm^{-1} of the strong absorption peaks. With the relatively high concentrations of Nd^{3+} and Cr^{3+} it is not surprising that some peak broadening and additional structure may be observed under high resolution [14]. Struve and Huber [17] interpret line broadening in $\text{Cr}^{3+}:\text{GSGG}$ as due to lattice sites occupied by ions of different ionic radii. The strongest transitions appearing in figures 1 and 2 have linewidths at half-maximum less than 10 cm^{-1} at liquid helium temperature.

There is no absorption above the $[4I]15/2$ manifold until one reaches the manifolds of $[4F]3/2$ ($11,450\text{ cm}^{-1}$) (fig. 3), $[4F]5/2$ and $[2H]9/2$ ($12,500\text{ cm}^{-1}$), and $[4F]7/2$ and $[4S]3/2$ ($13,500\text{ cm}^{-1}$). The excited Stark levels for each of these manifolds have been identified from the liquid helium temperature spectrum (table 2). Temperature-dependent spectra were used to establish the ground state splitting of the $[4I]9/2$ manifold consistent (within a wavenumber) to the ground state splitting established from the temperature-dependent spectra of the $[4I]11/2$, $[4I]13/2$, and $[4I]15/2$ manifolds (table 1).

Absorption by Cr^{3+} appears near 7000 \AA ($14,200\text{ cm}^{-1}$). Only at liquid helium temperature are the details sharp enough to measure (table 3). The R_1 and R_2 peaks of the $[2E]$ state (levels 3 and 4 in fig. 4) are found at

6965 Å (14,354 cm⁻¹) and 6951 Å (14,382 cm⁻¹). Both peaks have a linewidth of 10 Å at half-maximum. R_2 (level 4) shows evidence of inhomogeneous line broadening (fig. 4). A band partially resolved into three peaks nearly as intense as the R_1 and R_2 peaks lies to the high-energy side of the R_2 peak. The peaks are at 6933 Å (14,420 cm⁻¹), 6923 Å (14,440 cm⁻¹), and 6909 Å (14,470 cm⁻¹). The onset of the first strong absorption band of Cr³⁺ begins around 6900 Å and shows a distinct shoulder near 6632 Å. This shoulder has structure with peaks at 6879, 6795, and 6776 Å (table 3). The band has a maximum absorbance at 6360 Å which decreases to the band edge at 5500 Å. Superimposed on the first Cr³⁺ band are the absorption peaks of the Nd³⁺ manifolds [4F]9/2 (fig. 4), [2H]11/2 (fig. 5), [2G]7/2, and [4G]5/2. Analysis of the absorption spectrum of Cr³⁺:GSGG (without Nd³⁺) and GSGG (without Cr³⁺ and Nd³⁺) allows one to separate spectral details of Cr³⁺ and Nd³⁺. The absorption spectrum of Cr³⁺:GSGG is displayed in figure 6.

Nd³⁺ absorption associated with the [4G]7/2, [2G]9/2, and [2K]13/2 manifolds appears near the onset of the second strong Cr³⁺ band beginning at 5150 Å. The Nd³⁺ energy levels for these states are listed in table 2. Near the beginning of the second band, Cr³⁺ peaks appear at 5043 and 4993 Å (table 3). These peaks have linewidths and line shapes similar to the R_2 and R_1 peaks. The second Cr³⁺ band is composed of two peaks at 4806 and 4540 Å. The band edge on the high-energy side is at 3900 Å. Superimposed on the second Cr³⁺ band are the Nd³⁺ spectra for the [4G]9/2, [4G]11/2, [2K]15/2, [2P]1/2, and [2D]5/2 manifolds. Table 2 presents the remaining energy levels for Nd³⁺, including those found on a third Cr³⁺ band beginning at 3400 Å (fig. 7). Cr³⁺ peaks identified from Cr³⁺:GSGG (no Nd³⁺) include 3665, 3438, 3431, 3425, and 3395 Å. The peaks have been confirmed by scanning the spectrum of the undoped crystal. Cr³⁺ absorption peaks on the third Cr³⁺ band are found at 3198, 3119, 3116, 3105, 3100, 3085, and 3081 Å (table 3). These peaks are weak in comparison with the strong sharp spectra of Gd³⁺ (fig. 8). Below 2800 Å the absorption of the crystal is too intense to permit observation of additional structure. Table 4 lists the energy levels of Gd³⁺ measured at three different temperatures. Even at room temperature it is possible to see all expected Stark levels resolved in each [6P]*J* manifold (fig. 8).

Table 1. Infrared energy levels: Nd³⁺

[SL]J	Label	Value of E (cm ⁻¹) at various temperatures ^a			Calculated E (cm ⁻¹) ^b	ΔE (cm ⁻¹) ^c
		RT	LN	LHe		
[4f]9/2 ^d 323 ^e	Z ₁	0	0	0	-1	-1
	Z ₂	105	106	106	106	0
	Z ₃	167	167	168	168	0
	Z ₄	263	264	...	265	...
	Z ₅	...	763 ^d	...	762	...
[4f]11/2 2182 ^e	Y ₁	1979	1979	1980	1981	1
	Y ₂	2002	2003	2004	2005	1
	Y ₃	2067	2067	2068	2066	-2
	Y ₄	2102	2102	2103	2103	0
	Y ₅	2383	2389	2391	2392	1
	Y ₆	2423	2430	2432	2432	0
[4f]13/2 4151 ^e	X ₁	3908	3908	3908	3908	0
	X ₂	3917	3917	3917	3918	1
	X ₃	4000	3999	4000	4000	0
	X ₄	4013	4011	4012	4009	-3
	X ₅	4352	4357	4359	4362	3
	X ₆	4363	4371	4372	4371	-1
	X ₇	4405	4411	4412	4412	0
[4f]15/2 6192 ^e	W ₁	5777	5777	5778	5778	0
	W ₂	5810	5813	5813	5812	-1
	W ₃	5910	5912	5913	5914	1
	W ₄	5947	5951	5954	5957	3
	W ₅	6493	6495	6497	6496	-1
	W ₆	6508	6510	6510	6510	0
	W ₇	6547	6553	6557	6557	0
	W ₈	6640	6642	6643	6642	-1

^aSpectra recorded using the FTIR spectrometer at room temperature (RT), liquid nitrogen (LN) temperature, and liquid helium (LHe) temperature. [4f]15/2 manifold recorded on spectrophotometer. Where data overlap, energy levels agree within 1 cm⁻¹.

^bCalculated energy levels based on B_{km} parameters appearing in table 6 under column 6, Nd³⁺(B).

^cDifference between calculated and observed levels at LHe temperatures.

^dFluorescence spectra at LN temperature [1] provide complete splitting of [4f]9/2 manifold as follows: Z₁ = 0, Z₂ = 107, Z₃ = 168, Z₄ = 263, Z₅ = 763, all in cm⁻¹.

^eTheoretical centroid in cm⁻¹.

Figure 1. Absorption spectrum of $[4f]11/2$ manifold of Nd^{3+} recorded at liquid helium temperature with FTIR spectrometer.

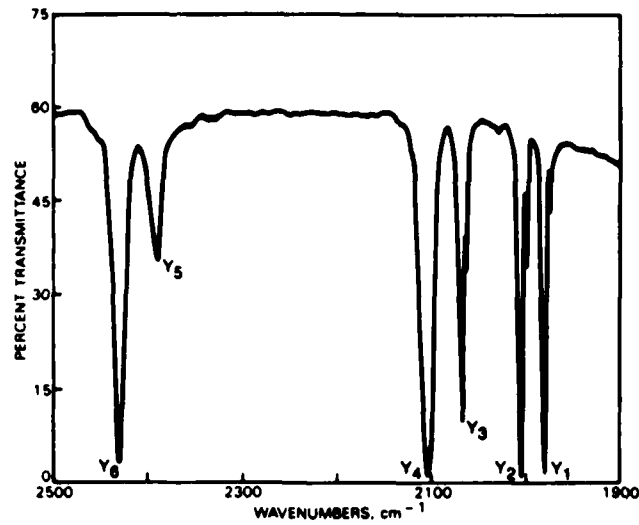


Figure 2. Absorption spectrum of $[4f]13/2$ manifold of Nd^{3+} recorded at liquid helium temperature with FTIR spectrometer.

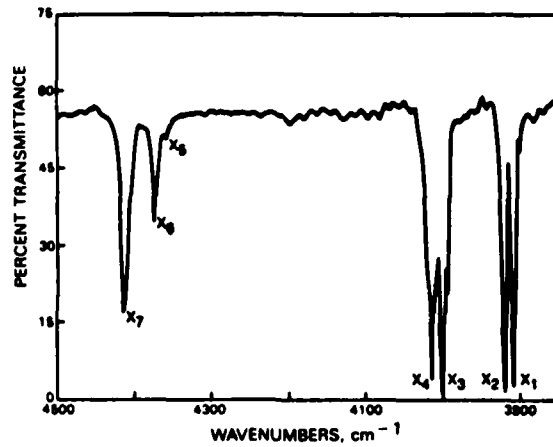


Figure 3. Absorption spectrum of $[4f]3/2$ manifold of Nd^{3+} recorded at room temperature showing temperature-dependent transitions from Stark levels Z_2 (106 cm^{-1}), Z_3 (167 cm^{-1}), and Z_4 (263 cm^{-1}) of ground state manifold $[4f]9/2$.

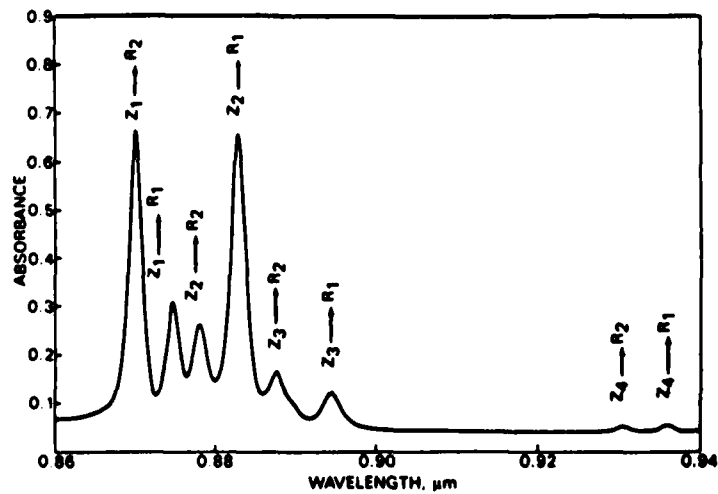


Table 2. Visible and ultraviolet energy levels: Nd³⁺

[SL]J	Label	Value of E (cm ⁻¹) at various temperatures ^a			Calculated E (cm ⁻¹) ^b	ΔE (cm ⁻¹) ^c
		RT	LN	LHe		
[4F]3/2	R ₁	11,431	11,432	11,432	11,432	0
11,497 ^d	R ₂	11,492	11,494	11,494	11,494	0
[4F]5/2	S ₁	12,350	12,352	12,354	12,348	-6
12,474 ^d	S ₂	12,395	12,390	12,390	12,392	2
[2H]9/2	S ₃	12,395	12,404	12,405	12,405	0
12,592 ^d	S ₄	12,540	12,543	12,544	12,544	0
	S ₅	12,580	12,584	12,586	12,590	4
	S ₆	12,610	12,617	12,618	12,618	0
	S ₇	12,743	12,745	12,745	12,746	1
	S ₈	12,790	12,791	12,793	12,791	-2
[4F]7/2	A ₁	13,372	13,374	13,374	13,375	1
13,455 ^d	A ₂	13,429	13,430	13,430	13,432	2
	A ₃	13,550	13,553	13,555	13,556	1
[4S]3/2	A ₄	13,560	13,566	13,566	13,567	1
13,547 ^d	A ₅	13,560	13,572	13,573	13,572	-1
	A ₆	13,608	13,610	13,611	13,609	-2
[4F]9/2	B ₁	14,634	14,637	14,639	14,641	2
14,724 ^d	B ₂	14,669	14,671	14,673	14,675	2
	B ₃	14,786	14,789	14,791	14,789	-2
	B ₄	14,804	14,806	14,810	14,809	-1
	B ₅	14,899	14,900	14,902	14,901	-1
[2H]11/2	C ₁	15,864	15,865	15,865		
	C ₂	15,888	15,890	15,890		
	C ₃	15,965	15,966	15,967		
	C ₄	16,086	16,090	16,091		
	C ₅	16,105	16,109	16,110		
[4G]5/2	D ₁	16,907	16,909	16,910		
	D ₂	17,000	17,005	17,008		
[2G]7/2	D ₃	...	17,020	17,022		
	D ₄	17,070	17,074	17,075		
	D ₅	17,278	17,282	17,284		
	D ₆	...	17,550	17,557		
	D ₇	17,563	17,570	17,573		

Table 2. Visible and ultraviolet energy levels: Nd³⁺ (cont'd)

[SL]J	Label	Value of E (cm ⁻¹) at various temperatures ^a			[SL]J	Label	Value of E (cm ⁻¹) at various temperatures ^a		
		RT	LN	LHe			RT	LN	LHe
[4G]7/2	E ₁	18,777	18,781	18,783	[2K]15/2	H ₅	21,778	21,780	21,783
	E ₂	18,864	18,864	18,864	(cont'd)	H ₆	21,884	21,884	21,885
	E ₃	18,881	18,883	18,884		H ₇	22,004	22,005	22,006
	E ₄	18,997	18,901	19,004		H ₈	22,053	22,054	22,054
[2K]13/2	F ₁	19,203	19,205	19,207	[2P]1/2	I ₁	23,190	23,192	23,193
	F ₂	19,236	19,238	19,238					
[2G]9/2	F ₃	19,330	19,334	19,335	[2D]5/2	J ₁	23,723	23,723	23,724
	F ₄	19,354	19,359	19,359		J ₂	23,778	23,779	3,780
	F ₅	19,410	19,411	19,412		J ₃	23,832	23,840	23,843
	F ₆	19,480	19,487	19,488	[2P]3/2	K ₁	26,045	26,046	26,047
	F ₇	19,518	19,520	19,521		K ₂	...	26,055	26,056
	F ₈	19,586	19,590	19,592					
	F ₉	19,615	19,619	19,620	[4D]3/2	L ₁	27,685	27,689	27,689
	F ₁₀	19,670	19,672	19,672		L ₂	27,761	27,765	27,765
	F ₁₁	19,820	19,824	19,824					
	F ₁₂	19,890	19,895	19,895	[4D]5/2	M ₁	27,880	27,880	27,882
						M ₂	28,035	28,039	28,040
	[4G]9/2	G ₁	20,793	20,795	20,797	[4D]1/2	M ₃	28,105	28,112
G ₂		20,824	20,828	20,828		M ₄	28,145	28,150	28,159
G ₃		20,842	20,845	20,846		M ₅	28,280	28,283	28,284
[4G]11/2	G ₄	20,852	20,856	20,858	[2J]11/2	M ₆	28,328	28,333	28,335
	G ₅	20,977	20,980	20,980		M ₇	28,409	28,413	28,413
	G ₆	21,040	21,042	21,043		M ₈	28,705	28,712	28,714
	G ₇	21,093	21,096	21,096		M ₉	28,853	28,857	28,859
	G ₈	21,143	21,145	21,146		M ₁₀	29,014	29,017	29,018
	G ₉	21,158	21,159	21,159					
	G ₁₀	21,203	21,206	21,207	[2L]15/2	N ₁	29,853	29,854	29,856
	G ₁₁	21,234	21,238	21,240		N ₂	29,963	29,960	29,958
						N ₃	29,969
	[2K]15/2	H ₁	21,609	21,610	21,611	[4D]7/2	N ₄	29,993	29,997
H ₂		21,714	21,714	21,714		N ₅	30,051	30,056	30,059
H ₃		21,740	21,740	21,742					
H ₄		21,772	21,773	21,774					

Table 2. Visible and ultraviolet energy levels: Nd³⁺ (cont'd)

[SL]J	Label	Value of E (cm ⁻¹) at various temperatures ^a			[SL]J	Label	Value of E (cm ⁻¹) at various temperatures ^a		
		RT	LN	LHe			RT	LN	LHe
[4D]7/2	N_6	...	30,070	30,073	[2L]17/2	O_1	31,413	31,413	31,414
(cont'd)	N_7	30,178	30,180	30,180		O_2	31,518	31,520	31,522
	N_8	30,209	30,210	30,210		O_3	31,568	31,570	31,570
	N_9	30,263	30,264	30,265		O_4	31,610	31,610	31,612
	N_{10}	30,300	30,306	30,308		O_5	31,660	31,662	31,662
	N_{11}	30,352	30,356	30,359		O_6	31,751	31,753	31,755
[2F]13/2	N_{12}	30,428	30,430	30,431	[2I]9/2	P_1	32,633	32,633	32,634
	N_{13}	30,453	30,453	30,454		P_2	32,684	32,686	32,686
	N_{14}	30,506	30,509	30,510		P_3	32,708	32,710	32,713
	N_{15}	30,532	30,536	30,540		P_4	32,770	32,772	32,774
	N_{16}	30,625	30,627	30,630		P_5	32,791	32,795	32,797

^aSpectra recorded on spectrophotometer at room temperature (RT), liquid nitrogen (LN) temperature, and liquid helium (LHe) temperature.

^bCalculated energy levels based on B_{km} parameters appearing in table 6 under column 6, Nd³⁺(B).

^cDifference between calculated and observed levels at LHe temperature; rms deviation for 45 levels (tables 1 and 2) is 1.7 cm⁻¹.

^dTheoretical centroid in cm⁻¹.

Table 3. Absorption spectra of Cr³⁺ at liquid helium temperature

<i>L</i>	λ (Å)	$\Delta\lambda^a$ (Å)	<i>I</i>	E_{obs} (cm ⁻¹)	E_{calc}^b (cm ⁻¹)	Rep ^c Γ_n	Free ion state ^d (%)
1	0	-37 ^e	4	100 ⁴ F
2	-37	6	100 ⁴ F
3	6965	10	0.15	14,354	15,296	6	85 ⁴ F + 9 ² G + 3 ² H
4	6951	10	0.19	14,382	14,328	4	94 ⁴ F + 4 ² G + 1 ² H
5	6933	8	0.15	14,420	14,436	4	79 ⁴ F + 13 ² G + 4 ² H
6	6923	10	0.14	14,440	14,480	6	87 ⁴ F + 8 ² G + 3 ² H
7	6909	10	0.12	14,470	14,486	4	100 ⁴ F
8	6879	5	0.02	14,533	14,540	4	96 ⁴ F + 2 ² G + 1 ² H
9	6795	10	0.04	14,714	14,831	6	45 ² G + 26 ⁴ F + 15 ² H
10	6776	5	0.03	14,754	14,842	4	44 ² G + 27 ⁴ F + 16 ² H
11	6632	8	0.03	15,074	15,176	6	39 ² G + 35 ² H + 19 ² P
12	6535	20	0.02	15,298	15,244	4	39 ² G + 33 ² H + 19 ² P
13	6360	500	0.43	15,719	15,421	4	38 ² G + 34 ² H + 23 ² P
14	5043	10	0.10	19,824	19,948	4	57 ⁴ F + 42 ⁴ P
15	4993	14	0.15	20,014	19,964	6	57 ⁴ F + 43 ⁴ P
16	4800	20	0.18	20,700	20,830	4	50 ⁴ F + 48 ⁴ P + 1 ² H
17	4806	100	0.45	20,800	20,861	6	50 ⁴ P + 49 ⁴ F
18	4783	sh ^f	...	20,900	20,881	4	50 ⁴ P + 49 ⁴ F
19	4772	...	0.50	20,950	20,901	4	51 ⁴ P + 49 ⁴ F
20	4650	sh ^f	...	21,500	21,532	4	33 ² H + 25 ² D1 + 19 ² D2
21	4540	100	0.45	22,020	22,014	6	40 ² H + 24 ² D1 + 17 ² D2
22	4524	sh ^f	0.49	22,100	22,063	4	39 ² H + 24 ² D1 + 17 ² D2
23	3665	10	0.01	27,277	27,185	4	100 ² G
24	3438	5	0.02	29,078	29,020	4	55 ² G + 39 ² H + 3 ² D2
25	3431	5	0.01	29,138	29,083	6	57 ² G + 37 ² H + 3 ² D2
26	3425	5	0.03	29,189	29,120	4	53 ² G + 43 ² H + 3 ² D2
27	3408	10	0.06	29,334	29,477	4	51 ² H + 29 ² G + 18 ² P
28	3395	7	0.02	29,447	29,592	4	51 ² H + 28 ² G + 20 ² P
29	29,602	6	50 ² H + 27 ² G + 21 ² P
30	31,258	4	47 ² H + 41 ² D2 + 8 ² D1
31	3198	10	0.01	31,261	31,259	6	48 ² H + 42 ² D2 + 8 ² D1
32	3119	5	0.04	32,052	32,068	4	50 ⁴ P + 49 ⁴ F
33	3116	...	0.04	32,082	32,087	6	49 ⁴ F + 49 ⁴ P + 1 ² H
34	3105	3	0.02	32,200	32,099	4	49 ⁴ F + 48 ⁴ P + 2 ² H
35	3100	10	0.07	32,249	32,107	4	50 ⁴ F + 48 ⁴ P + 1 ² H
36	3085	10	0.09	32,406	32,443	4	57 ⁴ P + 43 ⁴ F
37	3081	...	0.03	32,440	32,444	6	56 ⁴ P + 42 ⁴ F + 1 ² H

^aBandwidth: full width at half-maximum.

^bThe parameters (in cm⁻¹) used in the calculation are $F^{(2)} = 54,320$, $F^{(4)} = 43,094$, $\alpha = 2.88$, $\gamma = -63.28$, $\zeta_4 = 169.64$, $B_{20} = 1072$, $B_{40} = -22,251$, and $B_{43} = 23,443$, with an rms = 87.7 cm⁻¹. ($B = 620$, $C = 3420$, $Dq = 1450$, $v = -377.5$, $v' = 512.5$).

^cThe irreducible representations are $4 = \Gamma_4 + \Gamma_5$ and $6 = \Gamma_6$ (doublet) for the group C_3 or C_{3i} (all Γ_i and Γ'_i). The notation is from Koster et al [30].

^dOnly states of 1 percent or greater are listed.

^eThe splitting of the ground state is 0.235 cm⁻¹ with small amounts of the ⁴P and ²G mixed in.

^fShoulder of a band.

Figure 4. Absorption spectrum of Cr^{3+} levels 3 through 10 and the $[4F_{9/2}]$ manifold (B group) of Nd^{3+} recorded at liquid helium temperature.

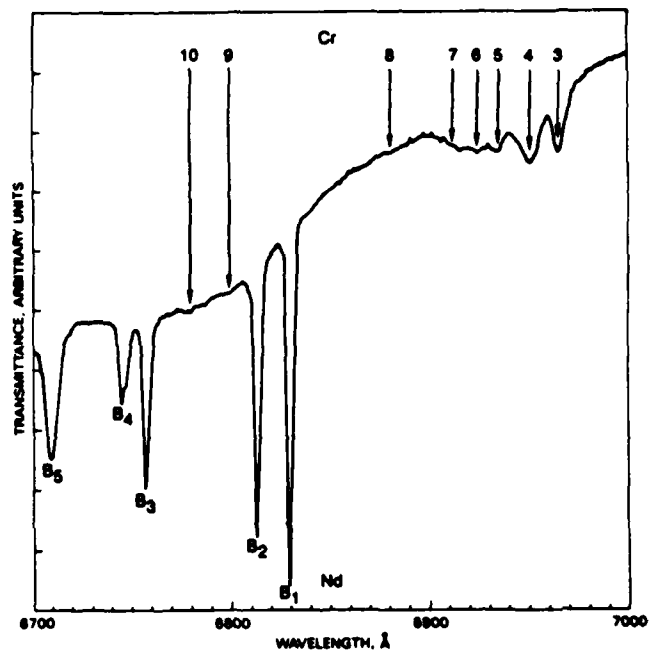


Figure 5. Absorption spectrum of $[2H_{11/2}]$ manifold of Nd^{3+} superimposed on first strong Cr^{3+} band, recorded at liquid helium temperature.

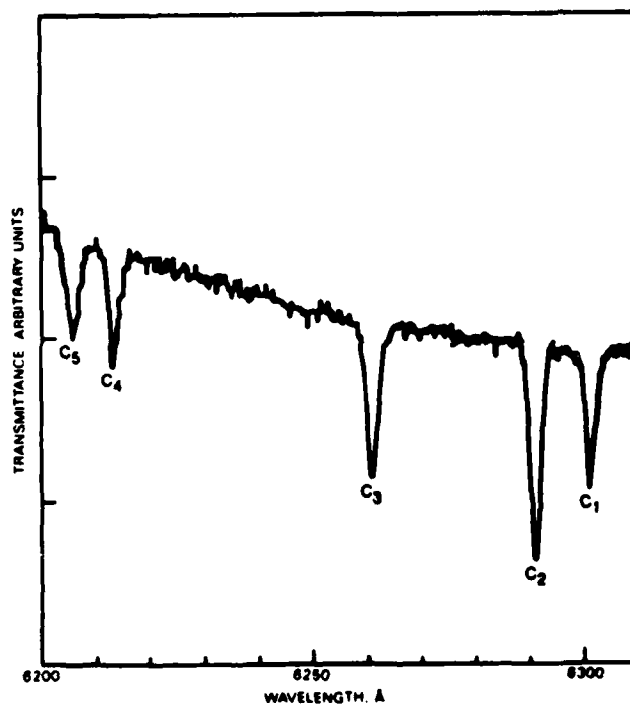


Figure 6. Absorption spectrum of $\text{Cr}^{3+}:\text{GSGG}$ between 3000 and 8000 Å recorded at room temperature with a Cary Model 17 spectrophotometer.

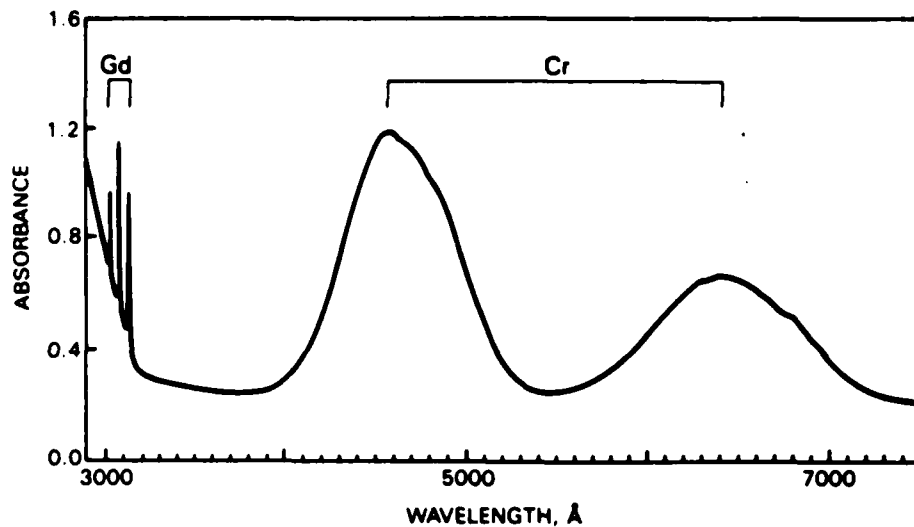


Figure 7. Absorption spectrum of $[4D]3/2$ (*L* group), $[4D]5/2$ and $[2I]11/2$ (*M* group), and part of $[4D]7/2$ and $[2I]13/2$ (*N* group) manifolds of Nd^{3+} superimposed on third Cr^{3+} band recorded at liquid helium temperature.

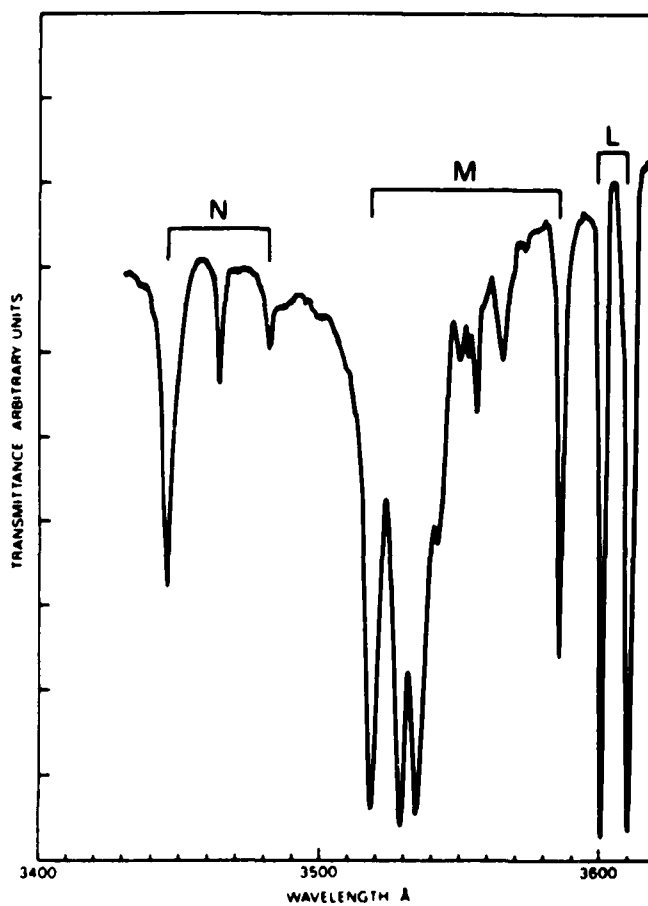


Figure 8. Absorption spectrum of $[6P]7/2$ (A group), $[6P]5/2$ (B group), and $[6P]3/2$ (C group) manifolds of Gd^{3+} recorded at room temperature.

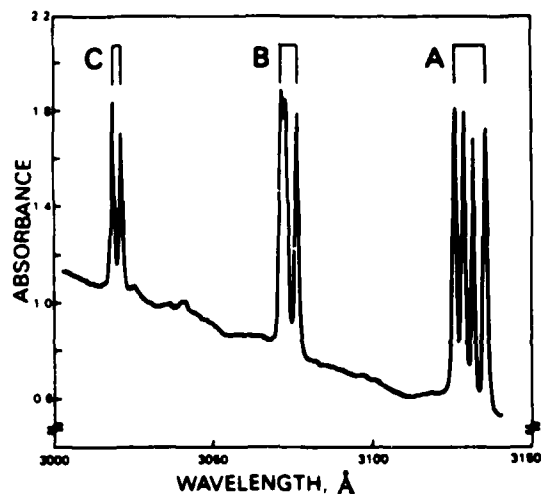


Table 4. Ultraviolet energy levels: Gd^{3+}

[SL]J	Label	Value of E (cm^{-1}) at various temperatures ^a			Calculated E (cm^{-1}) ^b	ΔE (cm^{-1}) ^c
		RT	LN	LHe		
[8S]7/2 0.4 ^d	Z_1	0	0	0	0.0	0
	Z_2	0.3	...
	Z_3	0.5	...
	Z_4	0.6	...
[6P]7/2 31,980 ^d	A_1	31,889	31,890	31,891	31,896	5
	A_2	31,926	31,927	31,927	31,922	-5
	A_3	31,958	31,960	31,961	31,966	5
	A_4	31,988	31,990	31,991	31,989	-2
[6P]5/2 32,573 ^d	B_1	32,499	32,501	32,503	32,506	3
	B_2	32,536	32,534	32,532	32,528	-4
	B_3	32,548	32,549	32,551	32,556	5
[6P]3/2 33,156 ^d	C_1	33,090	33,092	33,093	33,093	0
	C_2	33,118	33,119	33,120	33,119	-1
[6I]7/2 35,879 ^d	D_1	35,860	35,857	-3
	D_2	35,892	35,889	-3
	D_3	35,900	35,901	1
	D_4	35,910	35,915	5

^aSpectra recorded on spectrophotometer at room temperature (RT), liquid nitrogen (LN) temperature, and liquid helium (LHe) temperature.

^bCalculated energy levels based on B_{km} parameters appearing in table 6.

^cDifference between calculated and observed levels at LHe temperature; rms deviation for 14 levels is 4 cm^{-1} .

^dTheoretical centroid in cm^{-1} .

3.2 Crystal-Field Splitting Calculations: Nd³⁺, Gd³⁺

The material GSGG is a mixed garnet with the same crystal structure as Y₃Al₅O₁₂ (YAG) [21,22]. The cubic space group is *Ia3d* with site symmetries as follows: Gd(Nd), *D*₂; Sc(Cr), *C*_{3i}; Ga, *S*₄; and O, *C*₁. Crystallographic data are summarized in table 5.

The CEF splitting of the 4*f*^{*n*} [*SL*]*J* manifolds, assuming that Gd³⁺ and Nd³⁺ occupy sites of *D*₂ point symmetry, was analyzed by diagonalizing a parameterized Hamiltonian,

$$H_{D_2} = \sum_{km} B_{km} C_{km} \quad , \quad (1)$$

in a free-ion wave function basis involving the 11 lowest 4*f*³ [*SL*]*J* manifolds for Nd³⁺ and the 12 lowest 4*f*⁷ [*SL*]*J* manifolds for Gd³⁺ [23]. Free-ion wave functions and reduced matrix elements of the *U*^(*k*) unit spherical tensors were first obtained by diagonalization of the free-ion Hamiltonian using parameters given by Carnall, Fields, and Rajnak [24]. The nine real, even-fold (even-*k*) parameters in the *D*₂ Hamiltonian were varied to obtain agreement with observed splitting. The relationship between the *B*_{*km*} parameters used in this study, along with the *A*_{*k*}^{*m*} (*r*^{*k*}) and *B*_{*km*} parameters which are frequently reported, and the six possible equivalent sets of *B*_{*km*} parameters for *D*₂ symmetry can be obtained by using the relations given elsewhere [14].

**Table 5. Crystallographic and x-ray data of Gd₃Sc₂Ga₃O₁₂^a
(Cubic *Ia3d*, 230, Z = 8)**

Ion	Site	Symmetry	x	y	z
Gd	24c	<i>D</i> ₂	0	1/4	1/8
Sc	16a	<i>C</i> _{3i}	0	0	0
Ga	24d	<i>S</i> ₄	0	1/4	3/8
O	96h	<i>C</i> ₁	-0.0272	0.0558	0.1501

^aLattice constant is *a* = 12.5668 Å from Brandle and Barns [38] and the fractional positions for the oxygen ions are for Y₃Ga₅O₁₂ from Euler and Bruce [39].

An initial set of phenomenological B_{km} parameters for Nd^{3+} was obtained from Morrison, Leavitt, and Gildner [23], who calculated the CEF splitting of the $[4I]J$ and $[4F]3/2$ manifolds using the data from Kaminskii et al [1]. The present paper extends that work by including data and calculations for the additional Nd^{3+} manifolds, $[4F]5/2$, $[2H]9/2$, $[4F]7/2$, $[4S]3/2$, and $[4F]9/2$. Table 6 presents the final set of B_{km} parameters based on the experimental energy levels listed in tables 1 and 2. The calculated splittings are also listed in tables 1 and 2. An rms deviation of 1.7 cm^{-1} is obtained for 45 observed levels using the final set of phenomenological B_{km} parameters under column Nd (B) (table 6).

The phenomenological B_{km} parameters were compared with those obtained from a lattice sum calculation by Morrison, Leavitt, and Gildner [23]. The fractional oxygen positions were taken from the isostructural material $\text{Y}_3\text{Ga}_5\text{O}_{12}$ [14]. Effective charges, Z_i ($q_i = eZ_i$) in units of the magnitude of the electric charge, were taken as $Z_{\text{Gd}^{3+}} = Z_{\text{Sc}^{3+}} = 3$, $Z_{\text{Ga}^{3+}} = 1$, and $Z_{\text{O}^{2-}} = -1.5$. The polarizability of oxygen, α_{O} , was taken as 0.244 \AA^3 . The resulting lattice sums, A_{km} , which include the point-charge, point-dipole, and self-induced contributions, are listed in table 6. The parameters A_{km} are related to the B_{km} phenomenological parameters through the expression

$$B_{km} = \rho_k(\text{Nd}) A_{km} \quad , \quad (2)$$

where $\rho_k(\text{Nd})$ are radial factors given by Morrison, Karayianis, and Wortman [25]. The lattice sum calculation predicts reasonable values for A_{km} considering the assumptions that have been made.

The set of B_{km} parameters for Gd^{3+} was obtained by using $\rho_k(\text{Gd})$ [25] and the phenomenological A_{km} lattice parameters from table 6. The number (14) of observed energy levels for Gd^{3+} is marginal for a meaningful analysis, when the symmetry is low and requires nine CEF parameters. The rms deviation for 14 observed levels is 4 cm^{-1} , which is within the uncertainty associated with the data recorded in the ultraviolet region.

Table 6. CEF parameters for Nd³⁺ and Gd³⁺

A_{km}	$A_{km}(\text{calc.})^a$ (cm ⁻¹ /Å) ^a	$A_{km}(\text{phenom.})^b$ Nd (cm ⁻¹ /Å) ^a	B_{km}	Nd ³⁺ (A) ^c (cm ⁻¹)	Nd ³⁺ (B) ^d (cm ⁻¹)	Gd ³⁺ ^e (cm ⁻¹)
A_{20}	3572	2544	B_{20}	434	416	154
A_{22}	1010	529	B_{22}	90	76	308
A_{40}	-8.19	-115	B_{40}	-67	-53	18
A_{42}	-3990	-3148	B_{42}	-1818	-1774	-1418
A_{44}	-2141	-1595	B_{44}	-921	-980	-699
A_{60}	-981	-934	B_{60}	-1485	-1516	-1043
A_{62}	-350	-427	B_{62}	-679	-671	-515
A_{64}	504	485	B_{64}	771	777	514
A_{66}	-337	-416	B_{66}	-661	-641	-693

^aTable 2, ref. 23.

^bValues of parameters A_{km} calculated from phenomenological B_{km} parameters given in ref. 23, an analysis of fluorescence data for [41]J and [41]3/2 manifolds reported in ref. 1.

^cInitial set of B_{km} parameters, from ref. 23.

^dFinal set of B_{km} parameters for Nd³⁺; 45 levels; rms deviation 1.7 cm⁻¹.

^e B_{km} parameters for Gd³⁺; 14 levels; rms deviation 4 cm⁻¹.

3.3 Crystal-Field Splitting Calculations: Cr³⁺

Since we have not previously given a detailed description of the method used to calculate the energy level and the fitting procedures used in the theory of transition-metal ions in solids, we go into some detail here. The free-ion interactions (H_{FI}) we include are as follows:

$$H_{FI} = \sum_{k=2,4} F^{(k)} \sum_{i>j} C_{kq}^*(i) C_{kq}(j) + \alpha L(L+1) + \gamma G(R_S) + \zeta_d \sum_{i=1}^N \vec{l}_i \cdot \vec{s}_i, \quad (3)$$

where $F^{(k)}$ are the Slater integrals, α and γ are parameters of the Trees interactions, and ζ_d is the spin-orbit constant. In equation (3), the Slater integrals are related to the Racah parameters by

$$\begin{aligned} F^{(2)} &= 7(7B + C) , \\ F^{(4)} &= 63C/5 , \end{aligned} \quad (4)$$

and the C_{kq} are related to the spherical harmonics by

$$\begin{aligned} C_{kq}(i) &= \sqrt{4\pi/(2k+1)} Y_{kq}(\theta_i, \phi_i) , \\ C_{k-q} &= (-1)^q C_{kq}^* . \end{aligned} \quad (5)$$

The quantity $G(R_5)$ is the Casimir operator for the rotation group R_5 , and the values for all the states of d^N are given by Judd [26]. For the Cr^{3+} free ion, the parameters in equation (3) have the following values from Uylings et al [27]: $F^{(2)} = 74,201$, $F^{(4)} = 45,822$, $\alpha = 29.87$, and $\zeta_d = 275$ (all in units of cm^{-1}).

Using equation (3) in a least-squares fit to the data reported by Sugar and Corliss [28], we obtained the following values: $F^{(2)} = 72,389$, $F^{(4)} = 43,044$, $\alpha = 91.75$, $\gamma = -129.6$, and $\zeta_d = 277.7$ (all in units of cm^{-1}).

The difference in the two sets of parameters is mostly because Uylings et al [27] include the Trees interaction with the parameter T as well as β , which multiplies the seniority operator. Because of the agreement given above for transition-metal ions in solids, equation (3) can be considered an adequate representation of the free-ion interaction.

For threefold symmetry such as is found at the Sc site in GSGG (see table 6), the crystal-field interaction (H_{CF}) is taken as

$$H_{CF} = B_{20} \sum_{i=1}^N C_{20}(i) + B_{40} \sum_{i=1}^N C_{40}(i) + B_{43} \sum_{i=1}^N [C_{4-3}(i) - C_{43}(i)] \quad , \quad (6)$$

where the B_{kq} are the crystal-field parameters and B_{43} can be chosen real and positive with no loss in generality. In the cubic approximation, $B_{20} = 0$ and $B_{43} = \sqrt{10/7} |B_{40}|$, and for this symmetry (threefold), $B_{40} = -14Dq$, where we assume Dq is a positive number.

The matrix elements of the Hamiltonian given in equations (3) and (6) were computed using tapes of coefficients of fractional parentage for the d^3 configuration. The notation of the free-ion levels is that of Nielson and Koster [29]. Total angular momentum wave functions are used; for C_3 symmetry the Γ_4 matrix elements [30] are obtained by choosing the projection M_J , as $M_J = 1/2 + 3q$, with q any integer and $|M_J| < J$. For the Γ_6 irreducible representation, again we have $M_J = 3/2 + 3q$, where q is any integer and $|M_J| < J$. With these values of M_J the basis is chosen as $[|JM_J\rangle + (-1)^{J-M_J}|J-M_J\rangle]/\sqrt{2}$ and the energy levels for the basis $[|JM_J\rangle - (-1)^{J-M_J}|J-M_J\rangle]/\sqrt{2}$ are identical. With these basis functions,

the matrices for the entire Hamiltonian are 39×39 for Γ_4 (Γ_5 is degenerate with Γ_4) and 21×21 for Γ_6 . No a priori assumptions are made concerning the relative strengths of the various terms in the Hamiltonian. This choice of basis, while not efficient for a cubic environment, avoids the tedious perturbation calculations when the ion is definitely not in a site of cubic symmetry.

Having established the method by which the calculations are made, we now turn briefly to describe the method used to establish the experimental energy levels. Since C_{3i} symmetry has inversion, pure electronic electric-dipole (zero-phonon) transitions are forbidden between states of the same parity. However, because the coupling between the lattice and the electronic states is so strong, the vibronic spectra are intense and represent most of the observed Cr^{3+} absorption spectra. The only exception is the observation of several allowed electronic magnetic-dipole transitions between Stark levels that are nearly 100-percent pure 4F states such as transitions between the ground state level and levels 3 and 4 (table 3).

At liquid helium temperature most of the temperature-dependent vibronic spectrum is diminished, so that if a zero-phonon or electronic transition were allowed, it would be found near the low-energy side of the observed vibronic spectra associated with an excited Stark level. Some years ago Satten and his coworkers were successful in analyzing the vibronic spectra, especially of octahedrally coordinated uranium complexes [31]. The method of analysis they used was adopted and expanded by others analyzing vibronic spectra of rare-earth ions having different symmetries [32]. Recently vibronic states in C_{3i} symmetry were analyzed and the electronic energy levels reported [33]. The method of analysis of vibronic spectra used here follows the detailed descriptions reported earlier. We conclude from our assignments that the uncertainty in location of isolated excited Stark levels is within the final rms value reported. The fluorescence spectrum observed at liquid helium temperature [17] also helps to establish the location of the levels. Several authors described the use of fluorescence data to establish electronic energy levels [14,17,31].

To determine approximate atomic parameters, we began by assuming cubic symmetry. From observed spectra, we estimated the position of the experimental centroids as ${}^4A_2 = 0$, ${}^2E = 14,368$, ${}^2T_1 = 14,436$, ${}^4T_2 = 14,793$, ${}^4T_1 = 20,330$, and ${}^4T_1 = 32,251$ (in cm^{-1}). In making these selec-

tions, we used a Tanabe plot [34] with $Dq = 1479.3$. This value of Dq gave $B_{40} = -20,710 \text{ cm}^{-1}$ and $B_{43} = 24,753 \text{ cm}^{-1}$. For free-ion parameters, we started with those of Cr^{3+} in $\text{Y}_3\text{Al}_5\text{O}_{12}$ (YAG) [35], which are $F^{(2)} = 55,800 \text{ cm}^{-1}$, $F^{(4)} = 36,800 \text{ cm}^{-1}$, and $\alpha = \gamma = \zeta_d = 0$. With the above parameters as starting values, a least-squares fit to the experimental centroids was performed. The resulting parameters obtained were $F^{(2)} = 50,200$, $F^{(4)} = 40,821$, $\alpha = 35.09$ ($\gamma = \zeta_d = B_{20} = 0$ not varied), $B_{40} = -20,797$, and $B_{43} = 24,857.71$ (in cm^{-1}). A similar fit to the limited data of Struve and Huber [17] gave $F^{(2)} = 53,961$, $F^{(4)} = 40,782$, $B_{40} = -21,882$, and $B_{43} = 26,154$ (in cm^{-1}) ($\alpha = \gamma = \zeta_d = B_{20} = 0$).

Proceeding now with the correct symmetry (C_{3i}) and the data given in table 5, we computed the point charge lattice sum parameters A_{nm} [23], which are $A_{20} = 812 \text{ cm}^{-1}/\text{\AA}^2$, $A_{40} = -11,413 \text{ cm}^{-1}/\text{\AA}^4$, and $A_{43} = 13,327 \text{ cm}^{-1}/\text{\AA}^4$. We then used the rotational invariants [36] defined here as

$$S_n(B) = \left[B_{n0}^2 + 2 \sum_{m>0}^n B_{nm}^* B_{nm} \right]^{1/2}, \quad (7)$$

which for C_{3i} symmetry gives

$$S_4(B) = [B_{40}^2 + 2B_{43}^2]^{1/2}. \quad (8)$$

If we assume the theoretical B_{nm} are given by $B_{nm} = \rho_n A_{nm}$, then $\rho_4 = S_4(B)/S_4(A)$. From equations (7) and (8) above we have

$$\rho_4 = 1.8537 \text{ \AA}^4. \quad (9)$$

If further we assume that $\rho_n = \langle r^n \rangle_{HF} / \tau^n$ (with $\langle r^n \rangle_{HF}$ given by a Hartree-Fock calculation and τ a radial expansion parameter), then we can write

$$\rho_2 = \langle r^2 \rangle_{HF} \sqrt{\rho_4 / \langle r^4 \rangle_{HF}}. \quad (10)$$

From Fraga et al [37] we have $\langle r^2 \rangle_{HF} = 0.4018 \text{ \AA}^2$ and $\langle r^4 \rangle_{HF} = 0.3344 \text{ \AA}^4$; therefore, $\rho_2 = 0.9460 \text{ \AA}^2$. Using the relation $B_{nm}^t = \rho_n A_{nm}$ and these values of ρ_2 and ρ_4 we have

$$\begin{aligned} B_{20}^t &= 786 \text{ cm}^{-1}, \\ B_{40}^t &= -21,156 \text{ cm}^{-1}, \\ B_{43}^t &= 24,704 \text{ cm}^{-1}. \end{aligned} \quad (11)$$

The crystal-field parameters given in equation (11) were then used as starting values along with the free-ion parameters obtained from fitting the experimental centroids and with $\zeta_d = 200 \text{ cm}^{-1}$ in a least-square fit to all the established energy levels. A total of 35 levels of Cr^{3+} were involved in the final analysis. The parameters obtained were $F^{(2)} = 54,320$, $F^{(4)} = 43,094$, $\alpha = 2.88$, $\gamma = -63.28$, $\zeta_d = 169.64$, $B_{20} = 1,072$, $B_{40} = -22,251$, and $B_{43} = 23,443$ (in cm^{-1}). The rms deviation is 87.7 cm^{-1} .

Table 3 gives the resulting energy levels, along with the percentage of the free-ion composition of each state (only values greater than 1 percent are given). The number of levels of the free-ion composition is limited to 3; the labels are in the convention of Nielson and Koster [29]. Because of the spin-orbit coupling and the twofold crystal field (B_{20}), the " 2E " cubic level becomes predominantly " 4F ," and the entire region from 14,300 through $15,000 \text{ cm}^{-1}$ is so mixed that a cubic interpretation is practically impossible.

4. Conclusions

From temperature-dependent absorption spectra of $\text{Nd}^{3+}:\text{GSGG}$ [1], $\text{Cr}^{3+}:\text{GSGG}$ [17], and $\text{Nd}^{3+}:\text{Cr}^{3+}:\text{GSGG}$ it has been possible to catalogue over 400 zero-phonon transitions which were used to establish the Stark levels of Nd^{3+} and Gd^{3+} ions occupying D_2 point symmetry in the lattice. The vibronic spectrum of Cr^{3+} in C_{3i} sites has been analyzed to establish the approximate location of many of the Stark levels of Cr^{3+} . A Hamiltonian consisting of Coulombic, spin-orbit, and CEF terms and having symmetry appropriate to each ion was diagonalized to obtain theoretical energy levels. The rms deviation between calculated and observed levels for Nd^{3+} (with 45 levels) is 1.7 cm^{-1} , for Gd^{3+} (with 14 levels) is 4 cm^{-1} and for Cr^{3+} (with 35 levels) is 87.7 cm^{-1} . The lattice sum calculations for both Nd^{3+} and Cr^{3+} are in reasonable agreement with the phenomenological parameters obtained from fitting the observed energy levels. The C_{3i} point symmetry of the lattice must be used to interpret the energy levels of Cr^{3+} in GSGG.

References

1. A. A. Kaminskii, Kh. S. Bagdasarov, G. A. Bogomolova, M. M. Gritsenko, A. M. Kevorkov, and S. E. Sarkisov, *Phys. Stat. Sol. (a)* **34** (1976), K 109.
2. B. Struve, G. Huber, V. V. Laptev, I. A. Shcherbakov, and E. V. Zharikov, *Appl. Phys. B* **28** (1982), 235; *B* **30** (1983), 117.
3. A. Beimowski, G. Huber, D. Pruss, V. V. Laptev, I. A. Shcherbakov, and E. V. Zharikov, *Appl. Phys. B* **28** (1982), 234.
4. D. Pruss, G. Huber, and A. Beimowski, *Appl. Phys. B* **28** (1982), 355.
5. E. V. Zharikov, V. V. Laptev, E. I. Sidorova, Yu. P. Timofeev, and I. A. Shcherbakov, *Sov. J. Quantum Electron.* **12** (1982), 1124.
6. E. V. Zharikov, N. N. Ill'ichev, V. V. Laptev, A. A. Malyutin, V. G. Ostroumov, P. P. Pashinin, and I. A. Shcherbakov, *Sov. J. Quantum Electron.* **12** (1982), 338.

7. E. V. Zharikov, N. N. Ill'ichev, S. P. Kalitin, V. V. Laptev, A. A. Malyutin, V. V. Osiko, V. G. Ostroumov, P. P. Pashinin, A. M. Prokhorov, V. A. Smirnov, A. F. Umyskov, and I. A. Shcherbakov, *Sov. J. Quantum Electron.* 13 (1983), 1274.
8. M. I. Demchouk, A. K. Gilev, A. M. Zabaznov, V. P. Mikhailov, A. A. Stavrov, and A. P. Shkadarevich, *Opt. Comm.* 55 (1985), 207.
9. E. Reed, *IEEE J. Quantum Electron.* QE-21 (1985), 1625.
10. M. Sekita, Y. Miyazawa, and S. Kimura, *J. Appl. Phys.* 58 (1985), 3658.
11. W. F. Krupke, M. D. Shinn, J. E. Marion, J. A. Caird, and S. E. Stokowskii, *J. Opt. Soc. Am. B* 3 (1986), 102. See also N. P. Barnes, D. J. Gettemy, L. Esterowitz, and R. E. Allen, *Comparison of Nd 1.06 and 1.33 μm Operations in Various Hosts*, *IEEE J. Quantum Electron.* QE-23 (1987), 1434; J. V. Meier, N. P. Barnes, D. K. Remelius, and M. R. Kokta, *IEEE J. Quantum Electron.* QE-22 (1986), 2058.
12. C. A. Morrison, *Application of Crystal-Field Theory to f^N and d^N Configurations*, Harry Diamond Laboratories, HDL-TR-2040 (1984).
13. J. B. Gruber, M. E. Hills, M. P. Nadler, M. R. Kokta, and C. A. Morrison, *Bull. Am. Phys. Soc.* 31 (1986), 243.
14. C. A. Morrison and R. P. Leavitt, *Spectroscopic Properties of Triply Ionized Lanthanides in Transparent Host Crystals*, in *Handbook on the Physics and Chemistry of Rare Earths*, V, ed. K. A. Gschneidner, Jr., and L. Eyring, North-Holland, New York (1982).
15. R. Reisfeld and C. K. Jorgensen, *Lasers and Excited States of Rare Earths*, Springer, New York (1977).
16. A. A. Kaminskii, *Laser Crystals*, Springer, New York (1981).
17. B. Struve and G. Huber, *Appl. Phys. B* 36 (1985), 195.

18. S. Sugano and Y. Tanabe, *J. Phys. Soc. Japan* *13* (1958), 880.
19. S. Sugano and I. Tsujikawa, *J. Phys. Soc. Japan* *13* (1958), 899.
20. M. O. Henry, J. P. Larkin, and G. F. Imbusch, *Proc. R. Ir. Acad.* *75* (1975), 97.
21. S. Geller, *Z. Kristallogr.* *125* (1967), 1.
22. G. I. Vetrogon, V. I. Danilenko, V. Ya. Kabanchenko, V. V. Osiko, A. M. Prokhorov, A. N. Terent'evskii, and M. I. Timoshechkin, *Sov. Phys. Solid State* *22* (1980), 1881.
23. C. A. Morrison, R. P. Leavitt, and M. D. Gildner, *Rare Earth Ion-Host Lattice Interactions: 15.--Analysis of the Spectra of Nd³⁺ in GSGG*, Harry Diamond Laboratories, HDL-TR-2035 (1984).
24. W. T. Carnall, P. R. Fields, and K. Rajnak, *J. Chem. Phys.* *49* (1968), 4412.
25. C. A. Morrison, N. Karayianis, and D. E. Wortman, *Rare Earth Ion-Host Lattice Interactions: 4.--Predicting Spectra and Intensities of Lanthanides in Crystals*, Harry Diamond Laboratories, HDL-TR-1816 (1977).
26. B. R. Judd, *Operator Techniques in Atomic Spectroscopy*, McGraw Hill, New York (1963), 162.
27. P.H.M. Uylings, A.J.J. Raassen, and J. F. Wyart, *J. Phys.* *B17* (1984), 4103.
28. J. Sugar and C. Corliss, *J. Phys. Chem. Ref. Data* *6* (1977), 137.
29. C. W. Nielson and G. F. Koster, *Spectroscopic Coefficients for the pⁿ, dⁿ, and fⁿ Configurations*, MIT Press, Cambridge, MA (1963).
30. G. F. Koster, J. O. Dimmock, R. G. Wheeler, and H. Statz, *Properties of the Thirty-Two Point Groups*, MIT Press, Cambridge, MA (1963).

31. R. A. Satten, *J. Chem. Phys.* *27* (1957), 286, and refs. therein.
32. W. E. Bron, *Phys. Rev.* *140* (1965), A2005, and refs. therein.
33. J. B. Gruber, R. P. Leavitt, C. A. Morrison, and N. C. Chang, *J. Chem Phys.* *82* (1985), 5373, and refs. therein.
34. Y. Tanabe and S. Sugano, *J. Phys. Soc. Japan* *11* (1956), 864.
35. D. T. Sviridov, R. K. Sviridova, N. I. Kulik, and V. B. Glasko, *J. Appl. Spectrosc.* *30* (1979), 334.
36. R. P. Leavitt, *J. Chem. Phys.* *7* (1982), 661.
37. S. Fraga, L.M.S. Saxena, and J. Karwowski, *Physical Science Data: 5. Handbook of Atomic Data*, Elsevier, New York (1976).
38. C. O. Brandle and R. L. Barns, *J. Crystal Growth* *20* (1979), 1.
39. F. Euler and J. A. Bruce, *Acta Cryst.* *19* (1965), 971.

DISTRIBUTION

ADMINISTRATOR
DEFENSE TECHNICAL INFORMATION CENTER
ATTN DTIC-DDA (12 COPIES)
CAMERON STATION, BUILDING 5
ALEXANDRIA, VA 22314

DIRECTOR
NIGHT VISION & ELECTRO-OPTICS LABORATORY
ATTN TECHNICAL LIBRARY
ATTN R. BUSER
ATTN A. PINTO
ATTN J. HABERSAT
FT BELVOIR, VA 22060

DIRECTOR
DEFENSE ADVANCED RESEARCH
PROJECTS AGENCY
ATTN J. FRIEBELE
1400 WILSON BLVD
ARLINGTON, VA 22209

DIRECTOR
DEFENSE NUCLEAR AGENCY
ATTN TECH LIBRARY
WASHINGTON, DC 20305

UNDER SECRETARY OF DEFENSE RES
& ENGINEERING
ATTN TECHNICAL LIBRARY, 3C128
WASHINGTON, DC 20301

OFFICE OF THE DEPUTY CHIEF OF STAFF,
FOR RESEARCH, DEVELOPMENT,
& ACQUISITION
DEPARTMENT OF THE ARMY
ATTN DAMA-ARZ-A, CHIEF SCIENTIST,
L. CAMERON
ATTN DAMA-ARZ-B, I. R. HERSHNER
WASHINGTON, DC 20310

COMMANDER
US ARMY ARMAMENT MUNITIONS &
CHEMICAL COMMAND (AMCCOM)
US ARMY ARMAMENT RESEARCH &
DEVELOPMENT CENTER
ATTN DRDAR-TSS, STINFO DIV
DOVER, NJ 07801

COMMANDER
ATMOSPHERIC SCIENCES LABORATORY
ATTN TECHNICAL LIBRARY
WHITE SANDS MISSILE RANGE, NM 88002

DIRECTOR
US ARMY BALLISTIC RESEARCH LABORATORY
ATTN DRDAR-TSB-S (STINFO)
ABERDEEN PROVING GROUND, MD 21005

DIRECTOR
US ARMY ELECTRONICS WARFARE LABORATORY
ATTN J. CHARLTON
ATTN DELET-DD
FT MONMOUTH, NJ 07703

COMMANDING OFFICER
USA FOREIGN SCIENCE & TECHNOLOGY CENTER
FEDERAL OFFICE BUILDING
ATTN DRXST-BS, BASIC SCIENCE DIV
CHARLOTTESVILLE, VA 22901

COMMANDER
US ARMY MATERIALS & MECHANICS
RESEARCH CENTER
ATTN DRXMR-TL, TECH LIBRARY
WATERTOWN, MA 02172

US ARMY MATERIEL COMMAND
5001 EISENHOWER AVE
ALEXANDRIA, VA 22333-0001

US ARMY MATERIEL SYSTEMS ANALYSIS
ACTIVITY
ATTN DRXSY-MP (LIBRARY)
ABERDEEN PROVING GROUND, MD 21005

COMMANDER
US ARMY MISSILE & MUNITIONS
CENTER & SCHOOL
ATTN ATSK-CTD-F
ATTN DRDMI-TB, REDSTONE SCI INFO CENTER
REDSTONE ARSENAL, AL 35809

COMMANDER
US ARMY RESEARCH OFFICE (DURHAM)
PO BOX 12211
ATTN ROBERT J. LONTZ
ATTN M. STOSIO
ATTN M. CIFTAN
ATTN B. D. GUENTHER
ATTN CHARLES BOGOSIAN
RESEARCH TRIANGLE PARK, NC 27709

COMMANDER
US ARMY RSCH & STD GRP (EUROPE)
FPO NEW YORK 09510

COMMANDER
US ARMY TEST & EVALUATION COMMAND
ATTN D. H. SLINEY
ATTN TECH LIBRARY
ABERDEEN PROVING GROUND, MD 21005

DISTRIBUTION (cont'd)

COMMANDER
US ARMY TROOP SUPPORT COMMAND
ATTN DRXRES-RTL, TECH LIBRARY
NATICK, MA 01762

OFFICE OF NAVAL RESEARCH
ATTN J. MURDAY
ARLINGTON, VA 22217

DIRECTOR
NAVAL RESEARCH LABORATORY
ATTN CODE 2620, TECH LIBRARY BR
ATTN CODE 5554, F. BARTOLI
ATTN CODE 5554, L. ESTEROWITZ
ATTN CODE 5554, R. E. ALLEN
WASHINGTON, DC 20375

HQ, USAF/SAMI
WASHINGTON, DC 20330

DEPARTMENT OF COMMERCE
NATIONAL BUREAU OF STANDARDS
ATTN LIBRARY
WASHINGTON, DC 20234

NASA LANGLEY RESEARCH CENTER
ATTN N. P. BARNES
HAMPTON, VA 23665

DIRECTOR
ADVISORY GROUP ON ELECTRON DEVICES
ATTN SECTRY, WORKING GROUP D
201 VARICK STREET
NEW YORK, NY 10013

AEROSPACE CORPORATION
PO BOX 92957
ATTN M. BIRNBAUM
ATTN N. C. CHANG
LOS ANGELES, CA 90009

COLORADO STATE UNIVERSITY
PHYSICS DEPARTMENT
ATTN S. KERN
FORT COLLINS, CO 80523

ALLIED
ADVANCED APPLICATION DEPT
ATTN A. BUDGOR
31717 LA TIEMDA DRIVE
WESTLAKE VILLAGE, CA 91362

AMES LABORATORY DOE
IOWA STATE UNIVERSITY
ATTN K. A. GSCHNEIDNER, JR. (2 COPIES)
AMES, IA 50011

ARGONNE NATIONAL LABORATORY
ATTN W. T. CARNALL
ATTN H. M. CROSSWHITE
9700 SOUTH CASS AVENUE
ARGONNE, IL 60439

ARIZONA STATE UNIVERSITY
DEPT OF CHEMISTRY
ATTN L. EYRING
TEMPE, AZ 85281

BRIMROSE CORP OF AMERICA
ATTN R. G. ROSEMEIER
7527 BELAIR ROAD
BALTIMORE, MD 21236

CARNEGIE MELLON UNIVERSITY
SCHENLEY PARK
ATTN PHYSICS & EE, J. O. ARTMAN
PITTSBURGH, PA 15213

ENGINEERING SOCIETIES LIBRARY
ATTN ACQUISITIONS DEPT
345 EAST 47TH STREET
NEW YORK, NY 10017

IBM RESEARCH DIVISION
ALMADEN RESEARCH CENTER
ATTN R. M. MACFARLANE
MAIL STOP K32 802(D)
650 HARRY ROAD
SAN JOSE, CA 95120

JOHNS HOPKINS UNIVERSITY
DEPT OF PHYSICS
ATTN B. R. JUDD
BALTIMORE, MD 21218

KALAMAZOO COLLEGE
DEPT OF PHYSICS
ATTN K. RAJNAK
KALAMAZOO, MI 49007

DIRECTOR
LAWRENCE RADIATION LABORATORY
ATTN MARVIN J. WEBER
ATTN HELMUT A. KOEHLER
ATTN W. KRUPKE
LIVERMORE, CA 94550

MARTIN MARIETTA
ATTN F. CROWNE
ATTN R. LEAVITT
ATTN J. LITTLE
ATTN T. WORCHESKY

DISTRIBUTION (cont'd)

MARTIN MARIETTA (cont'd)
ATTN D. WORTMAN
1450 SOUTH ROLLING ROAD
BALTIMORE, MD 21227

MASSACHUSETTS INSTITUTE OF TECHNOLOGY
CRYSTAL PHYSICS LABORATORY
ATTN H. P. JENSSEN
ATTN A. LINZ
CAMBRIDGE, MA 02139

MASSACHUSETTS INSTITUTE OF TECHNOLOGY
77 MASS AVE
ROOM 26-251
ATTN V. BAGNATO
CAMBRIDGE, MA 02139

MIT LINCOLN LAB
PO BOX 73
ATTN PETER MOULTON,
ATTN B. AULL
LEXINGTON, MA 02173

DEPARTMENT OF MECHANICAL, INDUSTRIAL,
& AEROSPACE ENGINEERING
PO BOX 909
ATTN S. TEMKIN
PISCATAWAY, NJ 08854

UNIVERSITY OF MICHIGAN
COLLEGE OF ENGINEERING NORTH CAMPUS
DEPARTMENT OF NUCLEAR ENGINEERING
ATTN CHIHIRO KIKUCHI
ANN ARBOR, MI 48104

NATIONAL OCEANIC & ATMOSPHERIC ADM
ENVIRONMENTAL RESEARCH LABS
ATTN LIBRARY, R-51, TECH RPTS
BOULDER, CO 80302

OAK RIDGE NATIONAL LABORATORY
ATTN R. G. HAIRE
OAK RIDGE, TN 37830

OKLAHOMA STATE UNIVERSITY
DEPT OF PHYSICS
ATTN R. C. POWELL
STILLWATER, OK 74078

PENNSYLVANIA STATE UNIVERSITY
MATERIALS RESEARCH LABORATORY
ATTN W. B. WHITE
ATTN B. K. CHANDRASEKHAR
UNIVERSITY PARK, PA 16802

SAN JOSE STATE UNIVERSITY
DEPARTMENT OF PHYSICS
ATTN J. B. GRUBER (10 COPIES)
SAN JOSE, CA 95192

SCIENCE APPLICATIONS, INC
ATTN T. ALLIK
1710 GOODRIDGE DRIVE
McCLEAN, VA 22102

SETON HALL UNIVERSITY
CHEMISTRY DEPARTMENT
ATTN H. BRITAIN
SOUTH ORANGE, NJ 07099

PRINCETON UNIVERSITY
DEPARTMENT OF CHEMISTRY
ATTN D. S. McCLURE
PRINCETON, NJ 08544

UNIVERSITY OF MINNESOTA, DULUTH
DEPARTMENT OF CHEMISTRY
ATTN L. C. THOMPSON
DULUTH, MN 55812

UNIVERSITY OF VIRGINIA
DEPT OF CHEMISTRY
ATTN DR. F. S. RICHARDSON (2 COPIES)
ATTN DR. M. REID
CHARLOTTESVILLE, VA 22901

UNION CARBIDE CORP
ATTN M. R. KOKTA (10 COPIES)
ATTN J. H. W. LIAW
750 SOUTH 32ND STREET
WASHOUGAL, WA 98671

COMMANDER
NAVAL WEAPONS CENTER
ATTN CODE 3854, R. SCHWARTZ
ATTN CODE 3854, M. HILLS (10 COPEIS)
ATTN CODE 3844, M. NADLER
ATTN CODE 385, R. L. ATKINS
ATTN CODE 343, TECHNICAL INFORMATION
DEPARTMENT
CHINA LAKE, CA 93555

AIR FORCE OFFICE OF SCIENTIFIC RESEARCH
ATTN MAJOR H. V. WINSOR, USAF
BOLLING AFB
WASHINGTON, DC 20332

US ARMY LABORATORY COMMAND
ATTN TECHNICAL DIRECTOR, AMSLC-CT

INSTALLATION SUPPORT ACTIVITY
ATTN LEGAL OFFICE, SLCIS-CC
ATTN S. ELBAUM, SLCIS-CC

USAISC
ATTN RECORD COPY, SLCIS-IM-TS
ATTN TECHNICAL REPORTS BRANCH,
ASNC-ADL-TR (3 COPIES)

DISTRIBUTION (cont'd)

HARRY DIAMOND LABORATORIES
 ATTN D/DIVISION DIRECTORS
 ATTN HDL LIBRARY, SLCHD-TL (3 COPIES)
 ATTN HDL LIBRARY, SLCHD-TL (WOODBIDGE)
 ATTN CHIEF, SLCHD-NW-E
 ATTN CHIEF, SLCHD-NW-EC
 ATTN CHIEF, SLCHD-NW-ED
 ATTN CHIEF, SLCHD-NW-EE
 ATTN CHIEF, SLCHD-NW-R
 ATTN CHIEF, SLCHD-NW-RA
 ATTN CHIEF, SLCHD-NW-RC
 ATTN CHIEF, SLCHD-NW-RE
 ATTN CHIEF, SLCHD-NW-RH
 ATTN CHIEF, SLCHD-NW-RI
 ATTN CHIEF, SLCHD-NW-P
 ATTN CHIEF, SLCHD-PO
 ATTN CHIEF, SLCHD-ST-C
 ATTN CHIEF, SLCHD-ST-RS
 ATTN CHIEF, SLCHD-ST-RA
 ATTN CHIEF, SLCHD-TT
 ATTN WALTER, S., SLCIS-CP-TD
 ATTN WILLIS, B., SLCHD-IT-EB
 ATTN ZABLUDOWSKI, B., SLCHD-IT-EB
 ATTN HERSHALL, P., SLCHD-MI-S
 ATTN KENYON, C. S., SLCHD-NW-EC
 ATTN MILETTA J. R., SLCHD-NW-EC
 ATTN MCLEAN, F. B., SLCHD-NW-RC
 ATTN SATTTLER, J., SLCHD-PO-P
 ATTN LIBELO, L., SLCHD-ST-AB
 ATTN BENCIVENGA, A. A., SLCHD-ST-AC

HARRY DIAMOND LABORATORIES (cont'd)
 ATTN SATTTLER, J., SLCHD-PO-P
 ATTN NEMARICH, J., SLCHD-ST-CB
 ATTN WEBER, B., SLCHD-ST-CB
 ATTN BAHDER, T., SLCHD-ST-RA
 ATTN BENCIVENGA, B. SLCHD-ST-RA
 ATTN BRODY, P., SLCHD-ST-RA
 ATTN BRUNO, J., SLCHD-ST-RA
 ATTN DROPKIN, H., SLCHD-ST-RA
 ATTN EDWARDS, A., SLCHD-ST-RA
 ATTN HALL, K., SLCHD-ST-RA
 ATTN HANSEN, A., SLCHD-ST-RA
 ATTN HAY, G., SLCHD-ST-RA
 ATTN KATZEN, E., SLCHD-ST-RA
 ATTN NEIFELD, R., SLCHD-ST-RA
 ATTN PENNISE, C., SLCHD-ST-RA
 ATTN SCHMALBACH, R., SLCHD-ST-RA
 ATTN SEMENDY, F., SLCHD-ST-RA
 ATTN SIMONIS, G., SLCHD-ST-RA
 ATTN SIMPSON, T., SLCHD-ST-RA
 ATTN STEAD, M., SLCHD-ST-RA
 ATTN STELLATO, J., SLCHD-ST-RA
 ATTN TOBIN, M., SLCHD-ST-RA
 ATTN TURNER, G., SLCHD-ST-RA (10 COPIES)
 ATTN WONG, B., SLCHD-ST-RA
 ATTN WORTMAN, D., SLCHD-ST-RA
 ATTN GARVIN, C., SLCHD-ST-RB
 ATTN GOFF, J., SLCHD-ST-RB
 ATTN MORRISON, C., SLCHD-ST-RA (20 COPIES)

END

DATE

FILMED

7-88

Dtic